Spatial and Seasonal Variations in C_3H_x Hydrocarbon Abundance in Titan's Stratosphere from Cassini CIRS Observations

Nicholas A Lombardo[a,b,*], Conor A Nixon[a], Richard K Achterberg[a,c], Antoine Jolly[d], Keeyoon Sung[e], Patrick G J Irwin[f], F Michael Flasar[a]

[a] *Planetary Systems Laboratory, Solar System Exploration Division, NASA Goddard Space Flight Center, 8800 Greenbelt Road, Greenbelt, MD, USA*
[b] *Center for Space Science and Technology, University of Maryland, Baltimore County, 1000 Hilltop Circle, Baltimore, MD, USA*
[c] *Department of Astronomy, University of Maryland College Park, College Park, MD, USA*
[d] *Laboratoire Interuniversitaire des Systemes Atmospheriques, Universite Paris Est, Creteil, France*
[e] *Jet Propulsion Laboratory, California Institute of Technology, Pasadena, CA, USA*
[f] *Department of Atmospheric, Oceanic, and Planetary Physics, Camden College, University of Oxford, Oxford, UK*

Abstract

Of the C_3H_x hydrocarbons, propane (C_3H_8) and propyne (methylacetylene, CH_3C_2H) were first detected in Titan's atmosphere during the Voyager 1 flyby in 1980. Propene (propylene, C_3H_6) was first detected in 2013 with data from the Composite InfraRed Spectrometer (CIRS) instrument on Cassini. We present the first measured abundance profiles of propene on Titan from radiative transfer modeling, and compare our measurements to predictions derived from several photochemical models. Near the equator, propene is observed to have a peak abundance of 10 ppbv at a pressure of 0.2 mbar. Several photochemical models predict the amount at this pressure to be in the range 0.3 - 1 ppbv and also show a local minimum near 0.2 mbar which we do not see in our measurements. We also see that propene follows a different latitudinal trend than the other C_3 molecules. While propane and propyne concentrate near the winter pole, transported via a global convective cell, propene is most abundant above the equator. We retrieve vertical abundances profiles between 125 km and 375 km for these gases for latitude averages between 60°S to 20°S, 20°S to 20°N, and 20°N to 60°N over two time periods, 2004 through 2009 representing Titan's atmosphere before the 2009 equinox, and 2012 through 2015 representing time after the equinox. Additionally, using newly corrected line data, we determined an updated upper limit for allene (propadiene, CH_2CCH_2), the isomer of propyne). The measurements we present will further constrain photochemical models, by refining reaction rates and the transport of these gases throughout Titan's atmosphere.

*Corresponding author: Nicholas Lombardo, nicholas.lombardo@nasa.gov

1. Introduction

Titan, the largest moon of Saturn, is thought to have many similarities to the Archean Earth, including an atmosphere dominated by N_2, significant quantities of CH_4. The surface mixing ratio is 5% measured by the Huygens GCMS Niemann et al. (2010), and decreasing with altitude into the stratosphere where it remains constant with altitude at 1-1.5% as measured in Lellouch et al. (2014) on Titan. Global haze layers which continually shroud Titan and may have occurred intermittently on Earth. While factors like temperature, sources of atmospheric CH_4, and minor atmospheric constituents vary between the two bodies, Titan remains a good analog for studying the atmosphere of the Archean Earth (Izon et al., 2017), (Arney et al., 2016).

The global haze on Titan is produced through photolysis of CH_4 as Saturn Magnetospheric Electrons and solar UV photons bombard the upper atmosphere. The products of this process -highly reactive CH_3^-, H^+, and N^+ ions, among others- may then react to form C_2H_6, C_2H_4, and other molecules. As this complex process continues, larger hydrocarbons (C_xH_y) and nitriles ($C_xH_y(CN)_z$) react further to give rise to the 'photochemical zoo' of molecules present in Titan's atmosphere (Yung et al., 1984; Wilson and Atreya, 2004).

Titan's 26.7° obliquity, comparable to the Earth's 23.5° obliquity, causes variations in the insolation of the moon over the course of a Titan year (about 29.5 Earth years). The resulting seasonal variations in the physical state of the atmosphere have been observed and modeled in Caldwell et al. (1992), Lebonnois et al. (2001), Jennings et al. (2012), Teanby et al. (2012), Vinatier et al. (2015), and Coustenis et al. (2016), among others, see review by (Horst, 2017). Noteworthy is the existence of a global circulation cell, which transports warm gases in the summer hemisphere towards the winter pole, where they subside lower into the stratosphere. This downward advection causes adiabatic warming in the winter stratosphere and entrains short-lived gases produced in the upper stratosphere, increasing their abundance lower in the atmosphere. As northern winter evolved to northern spring, this single circulation cell transformed into two circulation cells, upwelling near the equator and downwelling at both poles, as predicted in Hourdin et al. (2004) and observed in Vinatier et al. (2015). For additional explanation of Titan's atmospheric dynamics and chemistry, the reader is directed to (Müller-Woodarg et al., 2014) and (Brown et al., 2010).

Regarding the C_3 hydrocarbons, propane (C_3H_8) and propyne (C_3H_4) were initially detected in Titan's atmosphere after the 1980 Voyager 1 flyby (Hanel et al., 1981) through spectra acquired by the IRIS instrument. Abundances for propyne were first estimated by (Maguire et al., 1981) by comparing the strength of the 633 cm^{-1} Q-branch of propyne to the 721 cm^{-1} Q-branch of acetylene (also ethyne, C_2H_2), and estimated to be on the order of 3×10^{-8}. Propane was modeled in the same paper using a synthetic spectrum constructed for its ν_{21} band, and a disk averaged value of 2×10^{-5} was reported. These values were updated by Coustenis et al. (1989) to $4.4^{+1.7}_{-2.1}\times10^{-9}$ for propyne and $(7\pm4)\times10^{-7}$ for propane. Further weak bands of propane were detected by the Composite InfraRed Spectrometer (CIRS) aboard Cassini (Nixon et al., 2009). Over three decades later, CIRS spectra were used to make the first detection of C_3H_6 (Nixon et al., 2013), however an exact abundance could not be retrieved from modeling the spectra due to the lack of a spectral line list, although an abundance estimate was made by comparing the intensities of propene and propane lines, discussed more in Section 4.2.

Recent analyses have shown the abundance of propyne to vary strongly with season and latitude. Vinatier et al. (2015), using limb viewing observations, showed the vertical gradient of C_3H_4 increases dramatically over the mid northern latitudes as northern winter moves into northern spring and the polar vortex responds to the changing amount of sunlight. Coustenis et al. (2018), using nadir observations to probe abundance in a narrow altitude range in the low stratosphere, show a similar trend at latitudes closer to the pole, between 60° and 90° either side of the equator. In the same studies, propane was shown to have a more constant abundance in latitude and time, remaining constant within error bars near 1×10^{-6} throughout the stratosphere, with the exception near the winter pole, where it increases with altitude.

Two C_3 hydrocarbons have yet to be firmly detected on Titan, allene (CH_2CCH_2, isomer of propyne) and cyclopropane ($CH_2CH_2CH_2$, isomer of propene). There was a tentative detection of allene by Roe et al. (2011), however an accurate linelist was not available at the time of the study, thus the authors were not able to model the potential allene feature and confirm its detection. In this paper, we discuss members of the C_3H_x series known to be present in Titan's atmosphere- propane (C_3H_8), propene (C_3H_6), and propyne (CH_3C_2H). We also searched for allene and provide an new upper limit for allene in regions close to the equator. This work was enabled by the creation of a propene pseudo-line list for Titan (Sung et al., 2018) and an updated line list for allene (see Section 2.2).

We use spectra collected by the CIRS instrument to determine the abundance of propene in Titan's stratosphere. We show latitudinal and seasonal variation in the distribution of propene, propane and propyne. The large number of CIRS observations used allows us to vertically resolve the profile of each gas. We compare the values determined to those predicted by photochemical models of Hébrard et al. (2013), Li et al. (2015), Loison et al. (2015), and Krasnopolsky (2014).

2. Methods

2.1. Dataset

CIRS is a Fourier Transform infrared spectrometer, with three focal planes spanning the 10 cm^{-1} - 1500 cm^{-1} spectral region (Jennings et al., 2017). We use spectra acquired by Focal Plane 3 (FP3, 580 cm^{-1}-1100 cm^{-1}) and Focal Plane 4 (FP4, 1050 cm^{-1}-1500cm^{-1}), two parallel arrays of 10 detectors each. Limb observations were performed at a spectral resolution of 0.5 cm^{-1} at distances between 10^5 km and 2×10^5 km from Titan, during which time each focal plane was positioned normal to Titan's surface, such that each detector sampled a different altitude. The arrays were centered at 125 km for between one and two hours and were then moved away from Titan's surface to stare at a central altitude of 350 km for a similar amount of time. The footprint of each detector (the vertical resolution) on Titan's atmosphere varied between 27 km and 54 km depending on the distance to the moon. The size of the footprint was comparable to Titan's atmospheric scale height, and thus allows us to vertically resolve physical characteristics of the atmosphere.

The C_3H_6 ν_{19} band detected in Nixon et al. (2013) at 912.67 cm^{-1} sits between several C_2H_4 emissions, and on top of a broad C_3H_8 band. To increase S/N to the point where we can model this feature, we chose to combine data from several flybys of Titan that are comparable in temperature. This results in averaging data from between three and seven flybys (or between 187 and 728 spectra) per time-latitude bin on Titan. We use two time periods - the pre equinox time from 2005 through 2008 (just before the northern vernal equinox of August 2009) and the post equinox time 2012 through 2015. During the time just after the northern vernal equinox, Cassini was in a very low inclination orbit relative to Saturn. Limb observations on Titan were focused on the polar regions, as Cassini was able to view these regions of the atmosphere continuously during a Titan flyby. We therefore do not include data from just after the equinox, as no limb data exists for the latitude regions we model in this work. In each time span, we combine observations representative of three latitude regions - northern, equatorial, and southern.

In our averages, we include data from 20° to 60° for both hemispheres, and within 20° of the equator. The former two bins represent the midlatitudes, and the third bin represent the equatorial atmosphere. While the latitude boundaries for observations we include are the same before and after equinox, the physical distribution of included observations varies. As an example, in the pre-equinox time, the northern bin contains observations from 24°N through 54°, whereas post-equinox we have observations only between 25°N and 48°N. The distribution of observations used is shown in Fig. 1 as black dots. The boundaries for each time-latitudinal bin are drawn as black boxes enclosing observations. We exclude observation centered at latitudes closer than 60° to either pole because temperature begins to vary strongly with latitude in these regions. Including these spectra in our averages would make the resultant spectra very difficult to model and obscure details of finer latitudinal variations in the retrieved profiles.

2.2. Spectral Line Data

Molecular line lists used were derived from the HITRAN (Gordon et al., 2017) and GEISA (Jacquinet-Husson et al., 2016) databases. The exceptions are propane (Sung et al., 2013), propene (Sung et al., 2018), propyne (previously used in in Coustenis et al. (2007)), diacetylene (Jolly et al., 2010), and allene, discussed below.

2.2.1. Updated Allene Linedata

No allene line lists are present either in HITRAN nor in GEISA but Coustenis et al. (1993) previously investigated the detectability of allene in Titan's atmosphere using spectroscopic parameters by Chazelas et al. (1985) for the ν_{10} band centered at 845 cm^{-1}. Line intensities were obtained from band intensity measurements by Koga et al. (1979). They concluded that the non-detection of allene implied an abundance below 5 ppbv.

In addition to this existing spectroscopic data, we include parameters obtained by high resolution studies (Hegelund et al., 1993) that address the existence of hot bands. The hot band contribution is necessary at room temperature to allow comparisons between these calculated line lists with observed room temperature spectra. Calculations were compared and validated against room and high temperature spectra taken at 0.08 cm^{-1} resolution in the ν_{10}/ν_9 wavenumber range (Es-sebbar et al., 2014). Comparisons between the calculated linelists and observed spectra are given in Jolly et al. (2015).

2.3. Radiative Transfer Modeling

Spectral fitting was done using the NEMESIS atmospheric modeling code (Irwin et al., 2008). NEMESIS operates on the method of optimal estimation, which involves the computation of a forward model and a retrieval process. The forward model was calculated using the correlated-k method of Lacis and Oinas (1991), and includes a Hamming apodization of Full Width at Half Maximum of 0.475 cm $^{-1}$ to recreate the instrument line shape. The retrieval process varies *a priori* profiles of chosen physical parameters to optimize the spectral fits. This is done by minimizing a cost-function which includes the deviation of the retrieved profile from the *a priori* estimate, and the quality of fit to the spectra (similar to a χ^2 goodness of fit test). NEMESIS has been extensively used to determine atmospheric abundances in the outer solar system using IR spectra, and application to Titan is described in Teanby et al. (2007), Teanby et al. (2009b), and Cottini et al. (2012).

Spectral modeling proceeded in two steps: stratospheric temperatures during observations were extracted, then the abundances of trace gases were retrieved. First, the 1275 cm^{-1} - 1325 cm^{-1} region of the ν_4 band of methane was modeled to extract the stratospheric temperature profile. While we did not model the entire ν_4 band that extends from 1250 cm^{-1} - 1350 cm^{-1}, the region of the spectrum we modeled contains sufficient information to retrieve the temperatures in the altitude regions needed for modeling the trace gases. Temperature measurements proceeded by assuming a methane abundance of 1.41×10^{-2} above 140 km, consistent with previous measurements and models (Lellouch et al., 2014), (Wilson and Atreya, 2004)) and an abundance below 140 km derived from measurements by the Huygens descent profile (Niemann et al., 2010). The initial temperature profile was derived from the HASI temperature (Fulchignoni et al., 2005) profile, and a non-gray aerosol haze was also allowed to vary. This retrieved temperature was then fixed while gases in the FP3 spectral region were allowed to vary. In the 900 cm^{-1} - 930 cm^{-1} region, the Q branch of the ν_{21} band of propane at 922 cm^{-1}, the ν_{19} propene band at 912.5 cm^{-1}, and ν_7 lines of ethylene at 915.5 cm^{-1} and 922.5 cm^{-1} were modeled. In the 620 cm^{-1} - 640 cm^{-1} region, the propyne ν_9 band at 633 cm^{-1} and diacetylene ν_8 band at 628 cm^{-1} were modeled.

The *a priori* volume mixing ratios (VMRs) used were constant over our range of sensitive altitudes above 100 km and set to values comparable to those reported in previous literature including Coustenis et al. (2007), Vinatier et al. (2007), Coustenis et al. (2010), and Vinatier et al. (2015), and represent 'rough guesses' for the abundance of each molecule in both time spans. Though some molecules have been shown to have vertical gradient that changes with time, we chose to use a constant profile above saturation that is the same for both time spans as to not influence the results of our comparisons across latitude and time. The *a priori* value for propene is comparable to predictions from Hébrard et al. (2013), Nixon et al. (2013), Li et al. (2015), and Dobrijevic et al. (2016).

Gas	*a priori* VMR
C_2H_4	$(1.1\pm0.2)\times10^{-7}$
C_3H_8	$(1\pm0.5)\times10^{-6}$
C_3H_6	$(3\pm1.5)\times10^{-9}$
CH_3C_2H	$(1\pm0.4)\ \times10^{-8}$
C_4H_2	$(5\pm2.5)\times10^{-9}$

3. Results

Example spectra from the altitude bins used in the pre-equinox southern temperature retrieval are shown in Fig 2. Errors on the radiance were expanded to account for systematic uncertainties and prevent over-constraining the model. Normalized contribution functions - also called the inversion kernel are the rate of change of radiance with respect to abundance. Altitudes with higher values 'contribute' more to the calculated spectrum, and thus are the altitudes where the data give the most information - see Fig. 3. Retrieved temperature profiles for the pre-equinox time span and the post-equinox time span are shown in Fig. 4. We see variation in the stratospheric temperature and the shape and altitude of the stratopause as described in Flasar and Achterberg (2009). While the stratopause increases in altitude towards the north winter pole, we do not see the full extent of the stratopause, since our data is only sensitive to an altitude of 0.02 mbar. Contribution functions similar to Fig. 3 are shown in Fig. 5 for the propene retrieval. Figs. 6 and 7 show spectral fits for the pre-equinox southern bin, similar to those shown for temperature. The retrieved profiles of C_3H_4, C_3H_6, C_3H_8 are given in Fig. 8 and Fig. 9.

The C_3H_8 profile shows a peak stratospheric abundance at 0.5 mbar in the north during late winter, with the profile flattening out to a more vertically constant profile in the equatorial and southern bins. The post-equinox profiles show the peak altitude decreasing slightly in the north, and a similar peak at 0.7 mbar forming around the equator during early northern spring.

C_3H_6 does not follow the same trend as other C_3 hydrocarbons, the maximum abundance of the gas in both time seasons is above 1 mbar near the equator. This differs from the general trend of the other C3 hydrocarbons and trace gases, which tend to increase above the mid to high winter latitudes.

CH_3C_2H shows a nearly constant abundance within error bars in the northern pre-equinox bin, becoming more variable and decreasing in abundance as the latitude moves away from the winter pole. The CH_3C_2H abundance profiles for the post-equinox time span are comparable across latitudes. There appears to be some small but systematic error of the CH_3C_2H spectral fit that may require re-evaluation of the methylacetlyene line list. This misfit is also seen in Fig. 10 of Vinatier et al. (2007) and Fig. 12 of Coustenis et al. (2007).

4. Discussion

4.1. Propane

In the pre-equinox period, equatorial and southern propane increases with altitude from 5×10^{-7} at 10 mbar to 1×10^{-6} at 0.01 mbar. In the north (during winter at the time), the abundance achieves a maximum abundance of 1×10^{-6} at 0.3 mbar before it begins to decrease with altitude, returning the a similar abundance as in the southern ad equatorial regions. In the post-equinox period, the propane distribution remains largely unchanged within errorbars. The south shows the abundance around 1 mbar decrease from 1×10^{-6} to 8×10^{-7}, just outside of the errorbars on the retrieval.

We are able to compare to Vinatier et al. (2007), who measure abundance from the first flyby of Titan by Cassini, Tb on 13 December 2004, at 15 °S. They show propane increasing monotonically from 4×10^{-7}

at 4 mbar to 1×10^{-6} at 0.01 mbar, which has a slightly greater slope than our pre-equinox values. In comparison, Bampasidis et al. (2012) probe the lower stratosphere using nadir observations between 2006 and 2012, they show propane generally at an southern and equatorial abundance of 5×10^{-7} between 2006 and 2009, in agreement with our results. At 50°N, they retrieve an abundance near 2×10^{-6} , which is slightly higher than our values at the lowest altitudes, but agree with our limb sounding around 3 mbar. Vinatier et al. (2015) perform another analysis of chemical abundance during the northern spring, between 2009 and 2013. At 46°N in 2012, they show propane at 4×10^{-7} at 5 mbar increasing to 1×10^{-6} at 0.03 mbar. Because their analysis was done on a single observation, the errorbars presented are large, so it is hard to compare variations in the vertical profile with our results, however they do seem compatible.

4.2. Propyne

Propyne shows stronger seasonal variation than propane. In the pre-equinox period, our results show propyne having a weak vertical gradient from 8×10^{-9} at 8 mbar to just under 2×10^{-8} at 0.01 mbar in the south. The vertical gradient decreases near the equator, and becomes nearly vertical in the north, indicative of the effect of downward advection within the winter polar vortex on the abundance profiles of trace gases.. In the post-equinox period, the propyne profile become similar across all latitudes, increasing from 1×10^{-8} at 8 mbar to 2×10^{-8} at 0.01 mbar. Bampasidis et al. (2012) report similar values to ours for the 2006-2009 period for 50°N, 0°N, and 50°S. Vinatier et al. (2007) show a steeper vertical profile at 15°S than our results indicate. Their modeled profile begins at a slightly lower abundance at 1 mbar and is in agreement with our results at higher altitudes. This could be explained by our larger dataset including observations later in the season and at slightly higher latitudes, where we would expect to see more propyne at lower altitudes.

4.3. Propene

Photochemical models have included C_3H_6 beginning after the Voyager flyby (Yung et al., 1984). Since the start of the Cassini mission, several new models have also incorporated the molecule (Wilson and Atreya, 2004; Hébrard et al., 2013; **?**; Krasnopolsky, 2014; Li et al., 2015; Loison et al., 2015; Dobrijevic et al., 2016).

Yung et al. (1984) propose the main source of propene in Titan's stratosphere (<300 km) is from

$$C_2H_3 + CH_3 + M \rightarrow C_3H_6 + M.$$

Li et al. (2015) follow with additional production pathways

$$CH + C_2H_6 \rightarrow C_3H_6 + H,$$

dominating the region between 600 km and 1000 km, where CH molecules are plentiful and

$$C_3H_8 + h\nu \rightarrow C_3H_6 + H_2$$

dominating the region between 300 km and 600 km, where the pressure is not great enough for a termolecular reaction and CH is scarce. Alternatively, Hébrard et al. (2013) include

$$H + C_3H_5 \rightarrow C_3H_6$$

as the dominating production reactions at mid to high altitudes.

The first detection of C_3H_6 in Titan's atmosphere was made with the INMS instrument by Magee et al. (2009). However, because mass spectrometers can generally not differentiate between isomers, it is unknown whether this detection is of propene or cyclopropane. The first definitive detection of propene was made by Nixon et al. (2013) using an average of CIRS spectra between 30°S and 10°N from 1 July 2004 through 1 July 2010, similar to our 20°S-20°N pre-equinox bin. However, a spectral line list for propene did not exist at the time, so the gas could not be included in their radiative transfer calculations. Instead, estimates of abundance were made by comparing the relative intensities of the propane and propene lines, and they claimed a 3-σ abundance of $(2.0\text{-}4.6)\times10^{-9}$ between 100 and 200 km.

In Fig. 10, we compare the predicted propene profiles to the abundance we determined for the pre-quinox time span, centered on the equator. Of the models compared, Loison et al. (2015) shows the best agreement. The abundance below 6 mbar is within the errorbars of our measured values. Above that, our measurements are within the 90th percentile of modeled profiles (90th percentile being the region which encloses 90% of modeled profiles.) In all other cases, the predictions have a peak abundance at or below 1 mbar, ranging from 1 to 6 ppbv. Our profiles display a peak abundance of 10 ppbv at 0.1 mbar, higher in abundance and altitude than all of the compared profiles. The profiles from Li et al. (2015) and Krasnopolsky (2014) show good agreement in abundance below 1 mbar, but also display an inversion above 0.2 mbar that we do not see in our measurements. We also retrieve about twice as much propene compared to the values inferred from relative line strengths in Nixon et al. (2013).

A modified version of the Loison et al. (2015) model was used as the Dobrijevic et al. (2016) model. Since the two models have different predicted profiles for propene, we can look at the differences between the two models in attempt to isolate the factors that caused the abundance of propene to change. Dobrijevic et al. (2016) list the changes from Loison et al. (2015) as: limiting the modeled hydrocarbons at C_4 species, excluding high mass nitriles, reducing the number of isomers included, and not considering reactions with 'very small fluxes'. The authors checked the effects of these changes on species included in the model, and while no major change was reported for significant molecules, we do see that the changes applied in Dobrijevic et al. (2016) decrease the predicted abundance of propene and worsen the agreement between the Loison et al. (2015) and our measurements. Due to the large number of reactions included in both models, we are unable to say which of these changes has the greatest effect on the modeled abundance of propene.

4.4. Allene

The isomer of propyne, CH_2CCH_2 or allene, is also theorized to be produced in Titan's atmosphere (Yung et al., 1984; Li et al., 2015). Production pathways for allene (and propyne) include

$$CH + C_2H_4 \rightarrow C_3H_4$$

above 600 km, with

$$H + C_3H_5 \rightarrow C_3H_4 + H_2$$

and

$$CH_3 + C_3H_5 \rightarrow C_3H_4 + CH_4$$

dominating throughout the rest of the atmosphere.

The only potential detection of allene on Titan was made in Roe et al. (2011), however since the line list used in the authors' analysis was in significant disagreement with the potential observed allene lines this remains only a tentative detection. Other analyses of Titan's atmosphere to search for allene have resulted in many upper limits. Coustenis et al. (2003) claimed a 3-σ upper limit of 2 ppbv, derived from disk averaged spectra from the Infrared Space Observatory (ISO). Nixon et al. (2010) estimate a 3-σ upper limit of 0.3 ppbv at 25° N at 107 km, and 1.6 ppbv at 76° N, 224 km, using a method described in their paper. We update these upper limits using a corrected line list produced by us and included in our radiative transfer calculations.

The spectrum used in the model is an average of nadir observations between 30°S and 30°N, from 2004-2015. Nadir observations were used to take advantage of the lower noise compared to limb viewing, however the abundance of allene is likely to be very low at the altitudes that nadir observations are sensitive to. Fig. 11 shows the best fit spectrum overlayed on the observed spectrum. The contributions of allene are visible as spikes in the dotted-line residual.

We perform a $\Delta\chi^2$ analysis similar to that described in Teanby et al. (2007) and Nixon et al. (2010) and estimate a 2-σ upper limit of 1 ppbv at 150 km within 30° North and South of the equator. A retrieval was performed between 830 and 880 cm^{-1} including ethane and propane spectral data, as for the previously described retrievals. The χ^2 value for this retrieval was considered χ_0^2. The best-fit abundances of ethane and propane were then held constant and varying amounts of allene were added to the atmosphere model. A forward model was run at each allene abundance to calculate a modified chi-squared value (χ_m), the $\Delta\chi^2$ value was calculated to be χ_m^2 - χ_0^2. We plot the values of $\Delta\chi^2$ as a function of added allene in Fig. 12. Where the $\Delta\chi^2$ achieves a minimum value, we claim an upper limit with a confidence of $(\Delta\chi^2)^{1/2}$. The results are shown in Fig. 11 and Fig. 12. A major challenge to modeling this allene band is the overlap of the band with the band of ethane and the band of propane. The ethane band is very bright, as seen in Fig. 11. Therefore, relatively small discrepancies in the modeling and linelist of ethane propagate heavily through to measuring allene. The propane band also present in the region we modeled is very dim and broad, further increasing the difficulty of measuring allene in this region, since it contributes mostly to the continuum in this small spectral window.

5. Conclusion

In this work, we have determined the first abundance profiles of propene in Titan's atmosphere, enabling us to compare the mixing ratio and spatial distribution of this gas with other trace gases, as well as compare to predictions from existing photochemical models. In brief, we've shown:

1. propene is present in Titan's atmosphere at a mixing ratio between 4 and 10 ppbv in the stratosphere
2. the abundance of propene near the equator is consistent with predictions from the Loison et al. (2015) model, but other predictions show a local inversion centered around 0.1 mbar, and a generally lower abundance
3. contrary to other trace gases, propene does not show a poleward enhancement in the winter hemisphere equatorward of 60°. Instead, propene shows an increased abundance above the equator relative to either pole.

The results of our analysis will be useful in refining models of Titan's atmospheric chemistry and dynamics as discrepancies between observations and predictions show that current photochemical models do not accurately predict the production and destruction rates of the molecule. Propene's unique spatial trend will make it a useful constraint in global circulation and transport models, as it may be a good tracer for horizontal transport. Additionally, the polymerization of propene and other π-bond molecules may lead to the formation of aerosols (Teanby et al., 2009a; Trainer et al., 2013)

Our updated upper limit for allene, calculated using the corrected linelist will also help to constrain theoretical production rates of the currently undetected gas.

6. Acknowledgments

N.A.L., C.A.N., R.K.A., and F.M.F. were supported by the NASA Cassini Project for the research work reported in this paper. Part of the research was carried out at the Jet Propulsion Laboratory, California Institute of Technology, under a contract with the National Aeronautics and Space Administration.

7. References

Achterberg, R. K., Gierasch, P., Contrath, B., Flasar, F., Jennings, D. E., Nixon, C. A., Nov. 2014. Post-equinox Variations of Titan's Mid-stratospheric Temperatures from Cassini/CIRS Observations. In: AAS/Division for Planetary Sciences Meeting Abstracts. Vol. 46 of AAS/Division for Planetary Sciences Meeting Abstracts. p. 102.07.

Arney, G., Domagal-Goldman, S. D., Meadows, V. S., Wolf, E. T., Schwieterman, E., Charnay, B., Claire, M., Hebrard, E., Trainer, M. G., 2016. The pale orange dot: The spectrum and habitability of hazy archean earth. Astrobiology 16, 873 – 899.

Bampasidis, G., Coustenis, A., Achterberg, R. K., Vinatier, S., Lavvas, P., Nixon, C. A., Jennings, D. E., Teanby, N. A., Flasar, F. M., Carlson, R. C., Moussas, X., Preka-Papadema, P., Romani, P. N., Guandique, E. A., Stamogiorgos, S., 2012. Thermal and chemical structure variations in Titan's stratosphere during the Cassini mission. The Astrophysical Journal 760 (2), 144–152.

Brown, R., Lebreton, J. P., Waite, J. (Eds.), 2010. Titan from Cassini Huygens. Springer.

Caldwell, J., Cunnginham, C. C., Anthony, D., White, H. P., Groth, E. J., Hasan, H., Noll, K., Smith, P. H., Tomasko, M. G., Weaver, H. A., 1992. Titan: Evidence for seasonal change a comparison of Hubble Space Telescope and Voyager images. Icarus 96, 1–9.

Chazelas, J., Pliva, J., Valentin, A., Henry, L., 1985. Analysis of the v9/v10 band system of allene. Journal of Molecular Spectroscopy 110, 326–338.

Cottini, V., Nixon, C., Jennings, D., Anderson, C., Gorius, N., Bjoraker, G., Coustenis, A., Teanby, N., Achterberg, R., BeÌĄzard, B., de Kok, R., Lellouch, E., Irwin, P., Flasar, F., Bampasidis, G., 2012. Water vapor in Titan's stratosphere from Cassini CIRS far-infrared spectra. Icarus 220, 855–862.

Coustenis, A., Achterberg, R. K., Conrath, B. J., Jennings, D. E., Marten, A., Gautier, D., Nixon, C. A., Flasar, F. M., Teanby, N. A., Bézard, B., Samuelson, R. E., Carlson, R. C., Lellouch, E., Bjoraker, G. L., Romani, P. N., Taylor, F. W., Irwin, P. G., Fouchet, T., Hubert, A., Orton, G. S., Kunde, V. G., Vinatier, S., Mondellini, J., Abbas, M. M., Courtin, R., 2007. The composition of TitanâĂŹs stratosphere from Cassini/CIRS mid-infrared spectra. Icarus 189, 35–62.

Coustenis, A., Bézard, B., Gautier, D., 1989. Titan's atmosphere from Voyager infrared obsverations, i. the gas composition of Titan's equatorial region. Icarus 80, 54–76.

Coustenis, A., Encrenaz, T., Bézard, B., Bjoraker, G., Graner, G., Dang-Nhu, M., Arié, E., 1993. Modelling Titan's thermal infrared spectrum for high resolution space observations. Icarus 102, 240–260.

Coustenis, A., Jennings, D. E., Achterberg, R. K., Bampasidis, G., Lavvas, P., Nixon, C. A., Teanby, N. A., Anderson, C. M., Cottini, V., Flasar, F. M., 2016. Titan's temporal evolution in stratospheric trace gases near the poles. Icarus 270, 409–420.

Coustenis, A., Jennings, D. E., Achterberg, R. K., Bampasidis, G., Nixon, C. A., Lavvas, P., Cottini, V., Flasar, F. M., 2018. Seasonal evolution of titan's stratosphere near the poles. The Astrophysical Journal 854, L30–L37.

Coustenis, A., Jennings, D. E., Nixon, C. A., Achterberg, R. K., Lavvas, P., Sinatier, S., Teanby, N. A., Bjoraker, G. L., Carlson, R. C., Piani, L., Bampasidis, G., Flasar, F. M., Romani, P. N., 2010. Titan's trace gas composition from CIRS at the end of the the Cassini-Huygens prime mission. Icarus 207, 461 – 476.

Coustenis, A., Salama, A., Schulz, Ott, S., Lellouch, E., Encrenaz, T., Gautier, D., Feuchtgruberc, H., 2003. Titan's atmosphere from ISO mid-infrared spectroscopy. Icarus 161, 383–403.

Dobrijevic, M., Loison, J., Hickson, K., Gronoff, G., 2016. 1d-coupled photochemical model of neutrals, cations and anions in the atmosphere of Titan. Icarus 268, 313–339.

Es-sebbar, E., Jolly, A., Benilan, Y., Farooq, A., 2014. Quantitative mid-infrared spectra of allene and propyne from room to high temperatures. Journal of Molecular Spectroscopy 305, 10–16.

Flasar, F. M., Achterberg, R. K., 2009. The structure and dynamics of Titan's middle atmosphere. Philosophical Transactions of the Royal Society A 367, 649–664.

Fulchignoni, M., Ferri, F., Angrilli, F., Ball, A. J., Bar-Nun, A., Barucci, M. A., Bettanini, C., Bianchini, G., Borucki, W., Colombatti, G., Coradini, M., Coustenis, A., Debei, S., Falkner, P., Fanti, G., Flamini, E., Gaborit, V., Grard, R., Hamelin, M., Harri, A. M., Hathi, B., Jernej, I., Leese, M. R., Lehto, A., Stoppato, P. F. L., López-Moreno, J. J., Mäkinen, T., McDonnell, J. A. M., McKay, C. P., Molina-Cuberos, G., Neubauer, F. M., Pirronello, V., Rodrigo, R., Saggin, B., Schwingenschuh, K., Seiff, A., Simoes, F., Svedhem, H., Tokano, T., Towner, M. C., Trautner, R., Withers, P., Zarnecki, J. C., 2005. In situ measurements of the physical characteristics of Titan's environment. Nature 438, 785–791.

Gordon, I., Rothman, L., Hill, C., Kochanov, R., Y.Tan, Bernath, P., Birk, M., Boudon, V., Campargue, A., Chance, K., Drouin, B., Flaud, J.-M., Gamache, R., Hodges, J., Jacquemart, D., Perevalov, V., Perrin, A., Shine, K., Smith, M.-A., Tennyson, J., Toon, G., Tran, H., Tyuterev, V., Barbe, A., Császár, A., Devi, V., Furtenbacher, T., Harrison, J., Hartmann, J.-M., Jolly, A., Johnson, T., Karman, T., Kleiner, I., Kyuberis, A., Loos, J., Lyulin, O., Massie, S., Mikhailenko, S., Moazzen-Ahmadi, N., Müller, H., Naumenko, O., Nikitin, A., Polyansky, O., Rey, M., Rotger, M., Sharpe, S., Sung, K., Starikova, E., Tashkun, S., Auwera, J. V., Wagner, G., Wilzewski, J., Wcislo, P., S.Yu, Zak, E., 2017. The HITRAN2012 spectroscopic database. JQSRT 203, 3–69.

Hanel, R., Conrath, B., Flasar, F. M., Kunde, V., Maguire, W., Pearl, J., Pirraglia, J., Sameulson, R., Herath, L., Allison, M., Cruikshank, D., Gautier, D., Gierasch, P., Horn, L., Koppany, R., Ponnamperuna, C., 1981. Infrared observations of the Saturnian System from Voyager 1. Science 212, 192–200.

Hébrard, E., Dobrijevic, M., Loison, J. C., Bergeat, A., Hickson, K. M., Caralp, F., 2013. Photochemistry of C3Hp hydrocarbons in Titan's stratosphere revisited. Astronomy and Astrophysics 552.

Hegelund, F., Andresen, A., Koivisaari, M., 1993. A high resolution infrared study of the v9+v11-v11, v10+v11-v11 hot band system in allene. Journal of Molecular Spectroscopy 159, 230–248.

Horst, S. M., 2017. Titan's atmosphere and climate. JGR:Planets 122 (3), 432–482.

Hourdin, F., Lebonnois, S., Luz, D., Rannou, P., 2004. Titan's stratospheric composition driven by condensation and dynamics. Journal of Geophysical Research: Planets 109, E12005–E12020.

Irwin, P., Teanby, N., de Kok, R., Fletcher, L., Howett, C., Tsang, C., Wilson, C., Calcutt, S., Nixon, C., Parrish, P., 2008. The NEMESIS planetary atmosphere radiative transfer and retrieval tool. Journal of Quantitative Spectroscopy and Radiative Transfer 109, 1136–1150.

Izon, G., Zerkle, A. L., Williford, K. H., Farquhar, J., Poulton, S. W., Claire, M. W., mar 2017. Biological regulation of atmospheric chemistry en route to planetary oxygenation. Proceedings of the National Academy of Sciences 114 (13), E2571–E2579.

Jacquinet-Husson, N., Armante, R., Scott, N., Chédin, A., Crepeau, L., Boutammine, C., Bouhdaoui, A., Crevoisier, C., Capelle, V., Boonne, C., Poulet-Crovisier, N., Barbe, A., Benner, D. C., Boudon, V., Brown, L., Buldyreva, J., Campargue, A., Coudert, L., Devi, V., Down, M., Drouin, B., Fayt, A., Fittschen, C., Flaud, J.-M., Gamache, R., Harrison, J., Hill, C., Hodnebrog, O., Hu, S.-M., Jacquemart, D., Jolly, A., Jimenez, E., Lavrentieva, N., Liu, A.-W., Lodi, L., Lyulin, O., Massie, S., Mikhailenko, S., Muller, H., Naumenko, O., Nikitin, A., Nielsen, C., Orphal, J., Perevalov, V., Perrin, A., Polovtseva, E., Predoi-Cross, A., Rotger, M., Ruth, A., Yu, S., Sung, K., Tashkun, S., Tennyson, J., Tyuterev, V., Auwera, J. V., Voronin, B., Makie, A., 2016. The 2015 edition of the GEISA spectroscopic database. Journal of Molecular Spectroscopy 327, 31 – 72.

Jennings, D. E., Anderson, C. M., Samuelson, R. E., Flasar, F. M., Nixon, C. A., Kunde, V. G., Achterberg, R. K., Cottini, V., de Kok, R., Coustenis, A., Vinatier, S., Calcutt, S. B., 2012. Seasonal disappearance of far-infrared haze in Titan's stratosphere. The Astrophysical Journal Letters 754, L3 – L7.

Jennings, D. E., Flasar, F. M., Kunde, V. G., Nixon, C. A., Segura, M. E., Romani, P. N., Gorius, N., Albright, S., Brasunas, J. C., Carlson, R. C., Mamoutkine, A. A., Guandique, E., Kaelberer, M. S., Aslam, S., Achterberg, R. K., Bjoraker, G. L., Anderson, C. M., Cottini, V., Pearl, J. C., Smith, M. D., Hesman, B. E., Barney, R. D., Calcutt, S., Vellacott, T. J., Spilker, L. J., Edgington, S. G., Brooks, S. M., Ade, P., Schinder, P. J., Coustenis, A., Courtin, R., Michel, G., Fettig, R., Pilorz, S., Ferrari, C., 2017. Composite infrared spectrometer (CIRS) on Cassini. Applied Optics 56 (18), 5274 – 5294.

Jolly, A., Benilan, Y., Manceron, L., Kwabia-Tchana, F., Nixon, C., 2015. Search for evidence of allene on Titan with new spectroscopic data. In: EPSC Abstracts. Vol. 10. pp. EPSC2015–171.

Jolly, A., Fayt, A., Benilan, Y., Jacquemart, D., Nixon, C. A., Jennings, D. E., 2010. The v8 bending mode of diacetylene: from laboratory spectroscopy to the detection of 13C isotopologues in Titan's atmosphere. The Astrophysical Journal 714, 852–859.

Koga, Y., Kondo, S., Nakanagaand, T., Saeki, S., 1979. Infrared absorption intensities of allene. Journal of Chemical Physics 71, 2404–2411.

Krasnopolsky, V. A., 2014. Chemical composition of titan's atmosphere and ionosphere: Observations and the photochemical model. Icarus 236, 83–91.

Lacis, A., Oinas, V., 1991. A description of the correlated k distribution method for modeling nongray gaseous absorption, thermal emission, and multiple scattering in vertically inhomogeneous atmospheres. Journal of Geophysical Research 96, 9027–9063.

Lebonnois, S., Toublanc, D., Hourdin, F., Rannou, P., 2001. Seasonal variations of Titan's atmospheric composition. Icarus 152, 384–406.

Lellouch, E., Bezard, B., Flasar, F., Vinatier, S., Achterberg, R., Nixon, C., Bjoraker, G., Gorius, N., 2014. The distribution of methane in Titan's stratosphere from Cassini/CIRS observations. Icarus 231, 323 – 337.

Li, C., Zhang, X., Gao, P., Yung, Y., 2015. Vertical distribution of C3 hydrocarbons in Titan's atmosphere. The Astrophysical Journal Letters 803, L19 – L26.

Loison, J., Hébrard, E., Dobrijevic, M., Hickson, K., Caralp, F., Hue, V., Gronoff, G., Venot, O., Bénilan, Y., 2015. The neutral photochemistry of nitriles, amines and imines in the atmosphere of titan. Icarus 247, 218–247.

Magee, B. A., Waite, J. H., Mandt, K. E., Westlake, J., Bell, J., Gell, D. A., 2009. INMS-derived composition of Titan's upper atmosphere: Analysis methods and model comparison. Planetary and Space Science 57, 1895–1916.

Maguire, W. C., Hanel, R. A., Jennings, D. E., Kunde, V. G., Samuelson, R. E., 1981. C3H8 and C3H4 in Titan's atmosphere. Nature 292, 683–686.

Müller-Woodarg, I., Griffith, C. A., Lellouch, E., Cravens, T. E. (Eds.), 2014. Titan Interior, Surface, and Space Environment. Cambridge University Press.

Niemann, H. B., Atreya, S. K., Demick, J. E., Gautier, D., Haberman, J. A., Harpold, D. N., Kasprzak, W. T., Lunine, J. I., Owen, T. C., Raulin, F., 2010. Composition of titanâĂŹs lower atmosphere and simple surface volatiles as measured by the CassiniâĂŘHuygens probe gas chromatograph mass spectrometer experiment. Journal of Geophysical Research 115, E12006–E12028.

Nixon, C., Achterberg, R., Teanby, N., Irwin, P., Flaud, J.-M., Kleiner, I., Dehayem-Kamadjeu, A., Brown, L., Sams, R., Bézard, B., Coustenis, A., Ansty, T., Mamoutkine, A., Vinatier, S., Bjoraker, G., Jennings, D., Romani, P., Flasar, F. M., 2010. Upper limits for undetected trace species in the stratosphere of Titan. Faraday Discussions 147, 95.

Nixon, C., Jennings, D., Flaud, J.-M., Bézard, B., Teanby, N., Irwin, P., Ansty, T., Coustenis, A., Vinatier, S., Flasar, F., 2009. Titan's prolific propane: A Cassini CIRS perspective. Planetary and Space Science 57, 1573–1585.

Nixon, C. A., Jennings, D. E., Bézard, B., Vinatier, S., Teanby, N. A., Sung, K., Ansty, T. M., Irwin, P. G. J., Gorius, N., Cottini, V., Coustenis, A., Flasar, F. M., 2013. Detection of propene in Titan's atmosphere. The Astrophysical Journal Letters 776, L14 – L20.

Roe, H. G., Greathouse, T., Tokunaga, A., 2011. Update on the TEXES Titan mid-infrared spectral survey. In: EPSC-DPS Joint Meeting 2011. p. 1398.

Sung, K., Toon, G. C., Drouin, B. J., Mantz, A. W., Smith, M. A. H., 2018. FT-IR measurements of cold propene (C3H6) cross-sections at temperatures between 150 and 299K. Journal of Quantitative Spectroscopy and Radiative Transfer 213, 119–132.

Sung, K., Toon, G. C., Mantz, A. W., Smith, M. A. H., 2013. FT-IR measurements of cold C3H8 cross sections at 7-15 microns for Titan atmosphere. Icarus 226.

Teanby, N., de Kok, R., Irwin, P., 2009a. Small-scale composition and haze layering in titan's polar vortex. Icarus 204 (2), 645–657.

Teanby, N., Irwin, P., de Kok, R., Jolly, A., Bézard, B., Nixon, C., Calcutt, S., 2009b. Titan's stratospheric C2N2, C3H4, and C4H2 abundances from Cassini/CIRS far-infrared spectra. Icarus 202, 620–631.

Teanby, N., Irwin, P., de Kok, R., Vinatier, S., Bézard, B., Nixon, C., Flasar, F., Calcutt, S., Bowles, N., Fletcher, L., Howett, C., Taylor, F., 2007. Vertical profiles of HCN, HC3N, and C2H2 in Titan's atmosphere derived from Cassini/CIRS data. Icarus 186, 364–384.

Teanby, N. A., Patrick G. J. Irwin and, C. A. N., de Kok, R., Vinatier, S., Coustenis, A., Sefton-Nash, E., Calcutt, S. B., Flasar, F. M., 2012. Active upper-atmosphere chemistry and dynamics from polar circulation reversal on Titan. Nature 491, 732–735.

Trainer, M. G., Sebree, J. A., Yoon, Y. H., Tolbert, M. A., 2013. THE INFLUENCE OF BENZENE AS a TRACE REACTANT IN TITAN AEROSOL ANALOGS. The Astrophysical Journal 766 (1), L4–L9.

Vinatier, S., Bézard, B., Fouchet, T., Teanby, N., de Kok, R., Irwin, P. G. J., Conrath, B. J., Romani, P. N., Flasar, F. M., Coustenis, A., 2007. Vertical abundance profiles of hydrocarbons in Titan's atmosphere at 15S and 80N retrieved from Cassini/CIRS spectra. Icarus 188, 120–138.

Vinatier, S., Bézard, B., Lebonnois, S., Teanby, N. A., Achterberg, R. K., Gorius, N., Mamoutkine, A., Guandique, E., Jolly, A., Jennings, D. E., Flasar, F. M., 2015. Seasonal variations in Titan's middle atmosphere during the northern spring derived from Cassini / CIRS observations. Icarus 250, 95–115.

Wilson, E. H., Atreya, S. K., 2004. Current state of modeling the photochemistry of Titan's mutually dependent atmosphere and ionosphere. Journal of Geophysical Research 109.

Yung, Y. L., Allen, M., Pinto, J. P., 1984. Photochemistry of the atmosphere of Titan: Comparison between model and observations. The Astrophysical Journal Supplement Series 55, 465–506.

				FP3								
			2004-2009						2012-2015			
	60°S-20°S		20°S-20°N		20°N-60°N		60°S-20°S		20°S-20°N		20°N-60°N	
Avg Lat	42°S		0°N		43°N		60°S-20°S		1°N		34°N	
Altitude (km)	spectra	NESR	spectra	NESR	spectra	NESR	spectra	NESR	spectra	NESR	spectra	NESR
100-150	322	1.58	330	1.68	412	1.53	299	2.30	440	1.82	288	2.41
150-200	451	1.37	428	1.48	537	1.37	416	1.96	608	1.67	395	2.19
200-250	515	1.32	460	1.50	568	1.30	441	1.85	601	1.61	464	1.89
250-300	496	1.34	440	1.45	634	1.23	463	1.99	680	1.60	446	1.74
300-350	271	1.67	299	1.79	294	1.60	229	2.60	297	2.16	341	1.92
350-375	235	1.96	242	1.89	258	1.59	218	2.33	287	2.21	191	2.70

				FP4								
Altitude (km)	spectra	NESR	spectra	NESR	spectra	NESR	spectra	NESR	spectra	NESR	spectra	NESR
100-150	310	0.29	369	0.23	515	0.29	388	0.40	345	0.30	298	0.33
150-200	381	0.22	463	0.27	652	0.23	530	0.27	488	0.30	397	0.32
200-250	372	0.24	573	0.24	691	0.17	551	0.21	503	0.26	464	0.29
250-300	334	0.26	559	0.19	728	0.18	583	0.20	556	0.23	450	0.24
300-350	187	0.39	450	0.22	345	0.28	305	0.29	230	0.33	336	0.28
350-400	187	0.29	277	0.30	294	0.30	265	0.32	232	0.38	183	0.29

Table 1: Observations averaged. Listed are the middle altitude, number of spectra averaged, and the noise equivalent spectral radiance (NESR) for each altitude bin. NESRs have units of nW cm^{-2} sr^{-1} cm, and were derived from the standard deviation of the mean for each average, and were measured at 910 cm^{-1} for FP3, and 1280 cm^{-1} for FP4 .

List of Figures

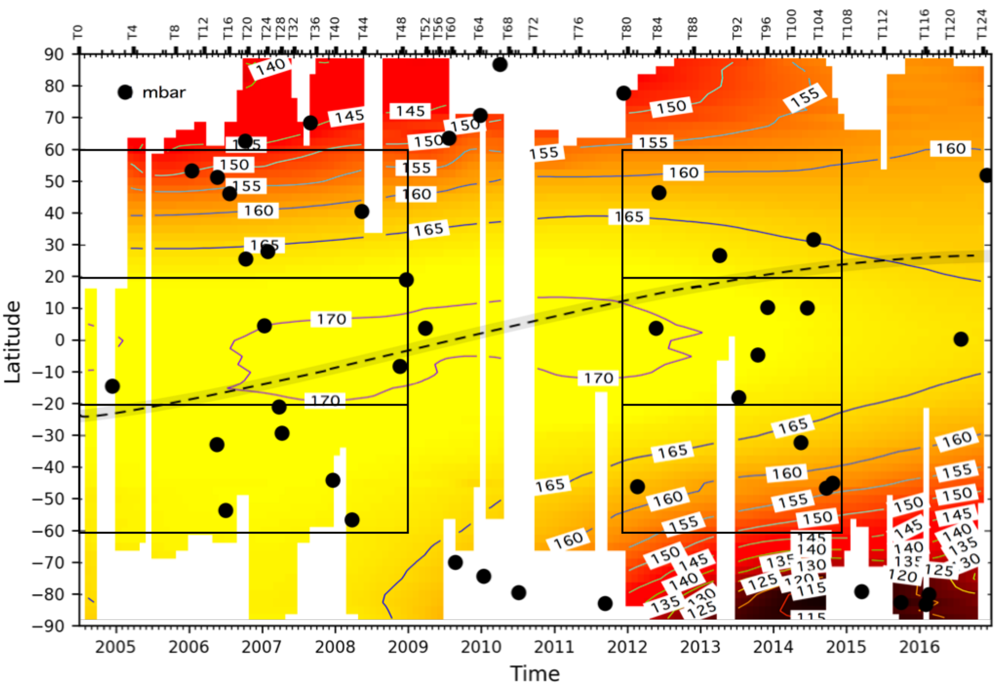

Figure 1: Distribution of all Mid-IR Limb Integrations (MIRLMBINT) observations during the Cassini mission shown as black circles. Temperatures are shown as contours (colored) and correspond to those at 1 mbar, or about 175 km, and are updated from Achterberg et al. (2014). The black boxes indicate the binning scheme with two time spans (2004-2009 and 2012-2015) further binned to three latitude ranges (60°S-20°S, 20°S-20°N, and 20°N-60°N). The dashed black line surrounded by gray is the solar latitude of Titan, where the Sun is directly overhead at 1200 local time.

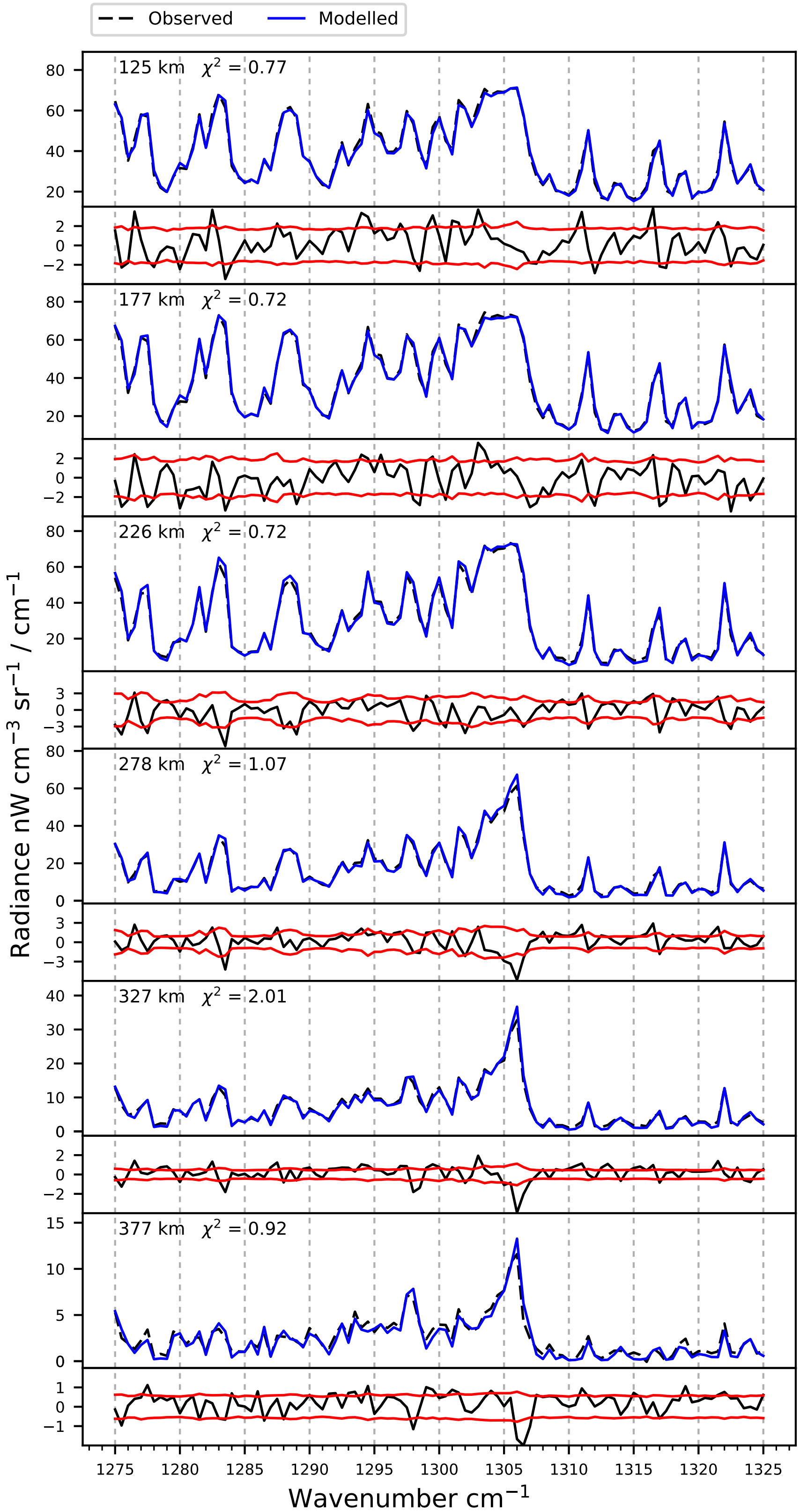

Figure 2: Spectra used in the 2004-2009 equatorial temperature retrieval of the methane ν_4 band. The altitude label corresponds to the peak contribution altitude, see Fig. 3

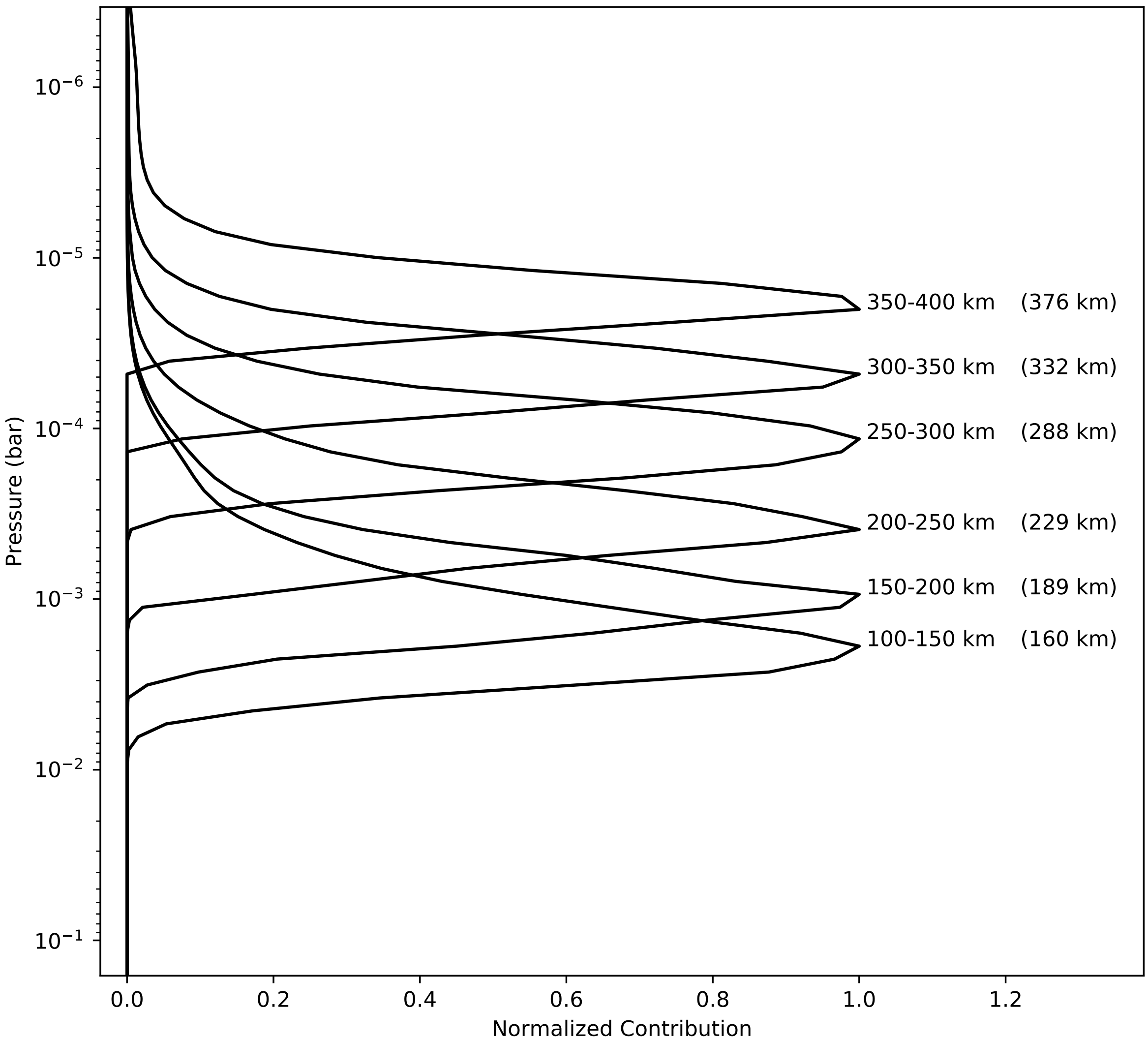

Figure 3: Normalized temperature contribution functions for each altitude bin, taken at 1311 cm^{-1}. Altitude bins are listed immediately to the right of each contribution function. The altitude where the contribution function peaks is listed in parantheses. In most cases, altitudes of peak contribution are not the center altitude for each bin.

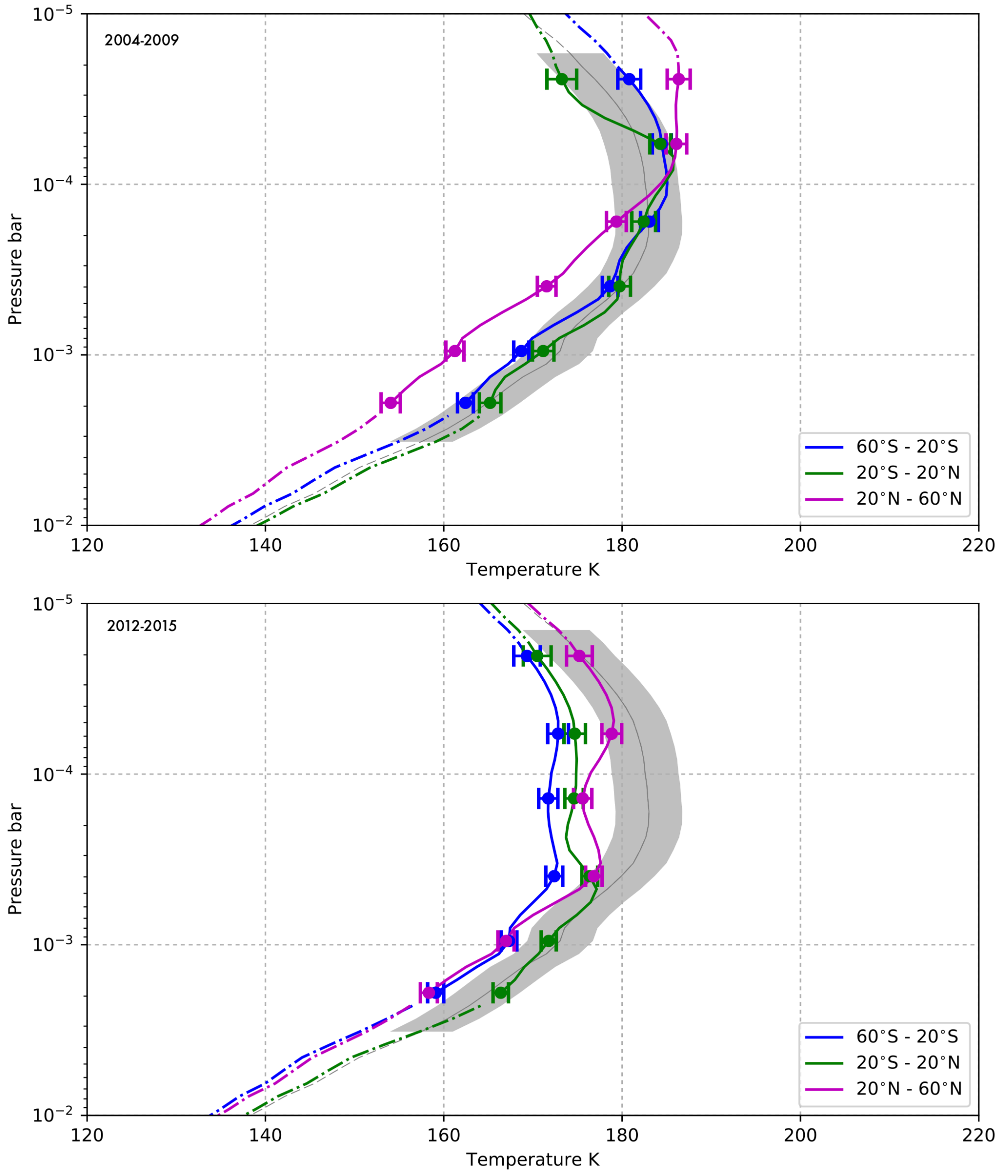

Figure 4: Comparison of retrieved temperatures in the 2012-2015 time span. 1-σ error bars are given at altitudes where the contribution function peaks in each altitude bin. The solid gray line is the a priori profile with error envelope. Dot dashed lines are the retrieved profile where there are no spectra.

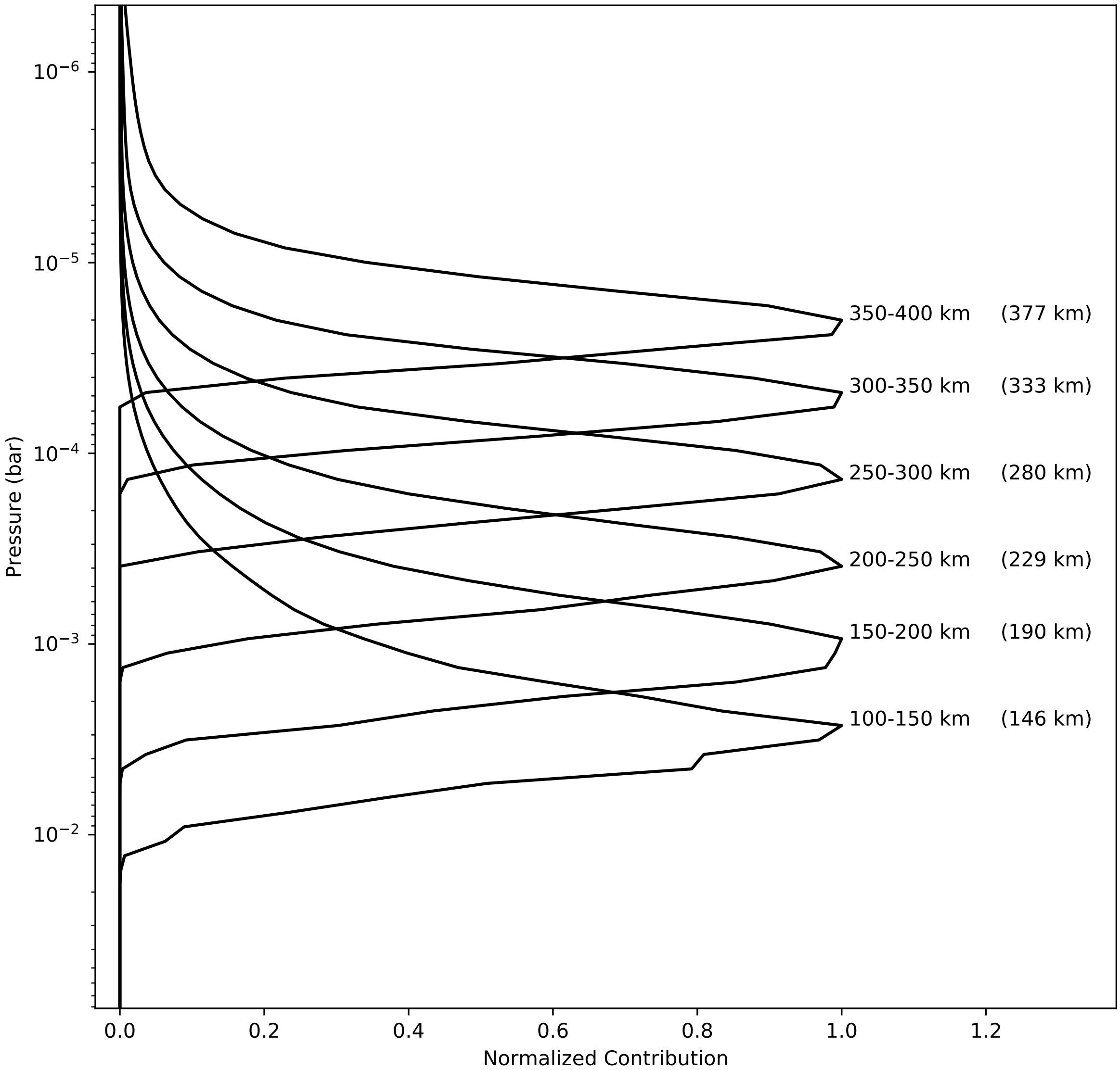

Figure 5: Normalized propene contribution functions for each altitude bin, taken at 912.5 cm^{-1}. Altitude bins are listed immediately to the right of each contribution function. The altitude where the contribution function peaks is listed in parantheses. In most cases, altitudes of peak contribution are not the center altitude for each bin.

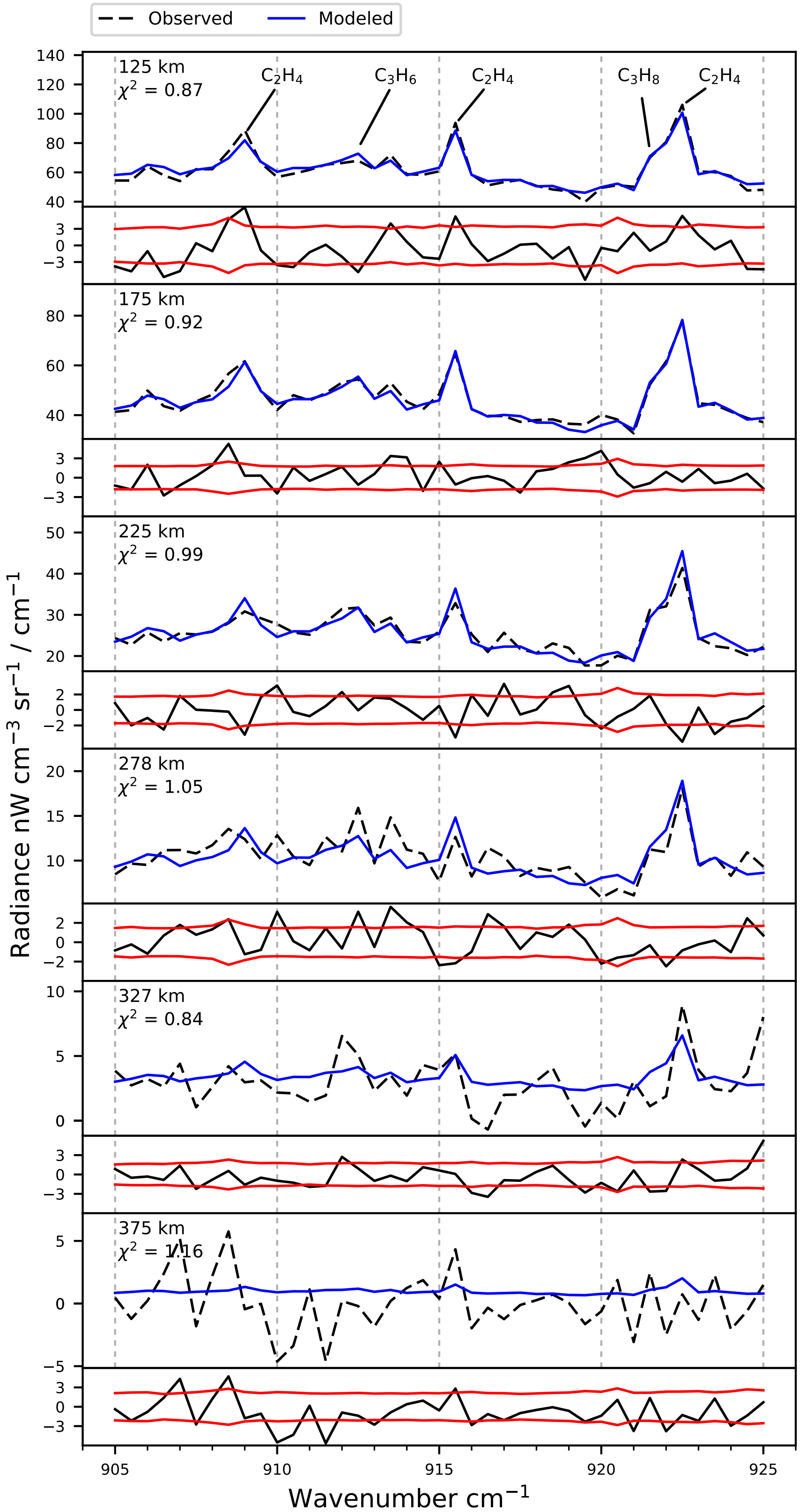

Figure 6: Spectral fits for propene and propane for the 2004-2009 time span in the equatorial bin.

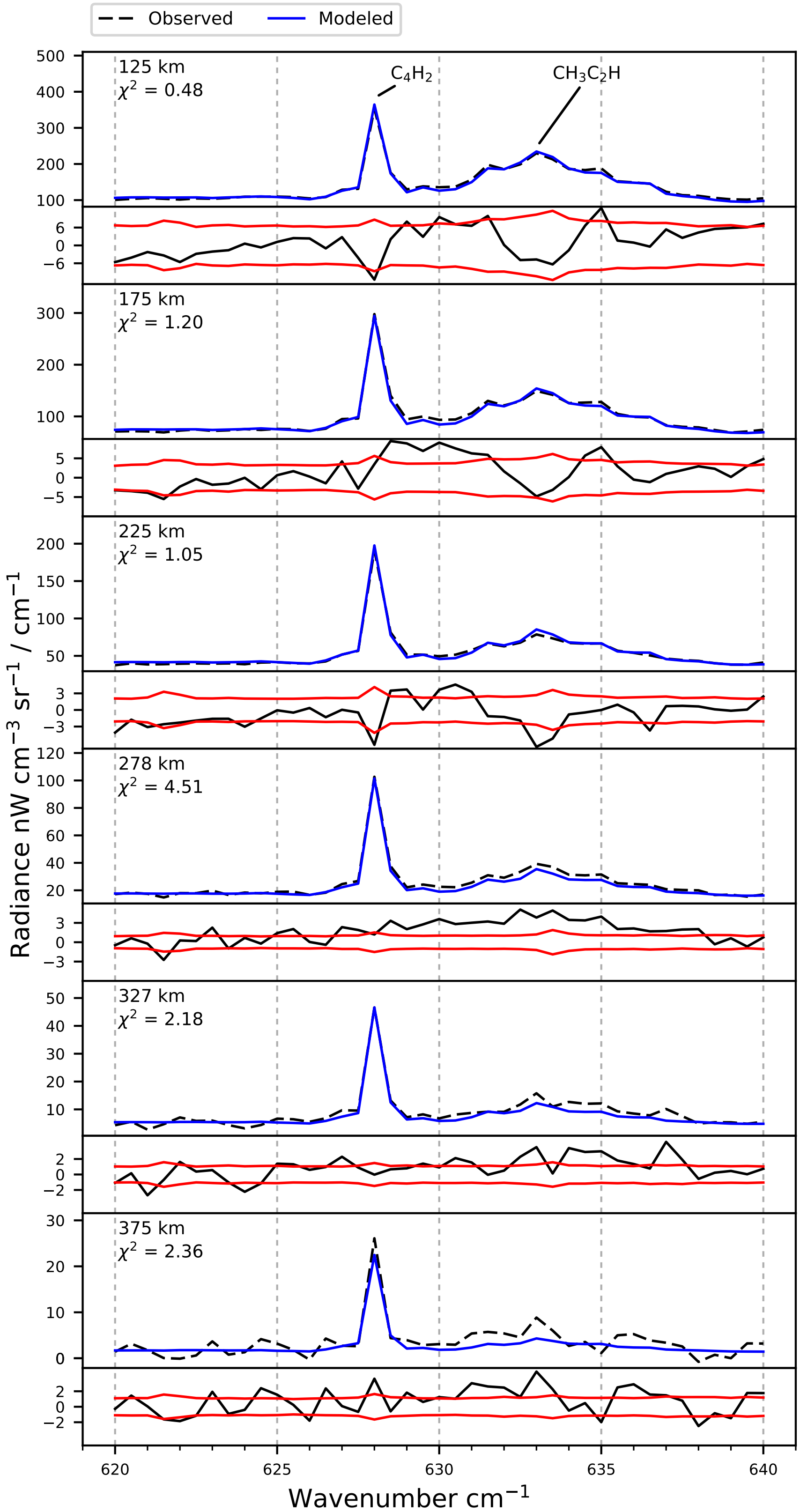

Figure 7: Spectral fits used in the 2004-2009 south propyne retrieval.

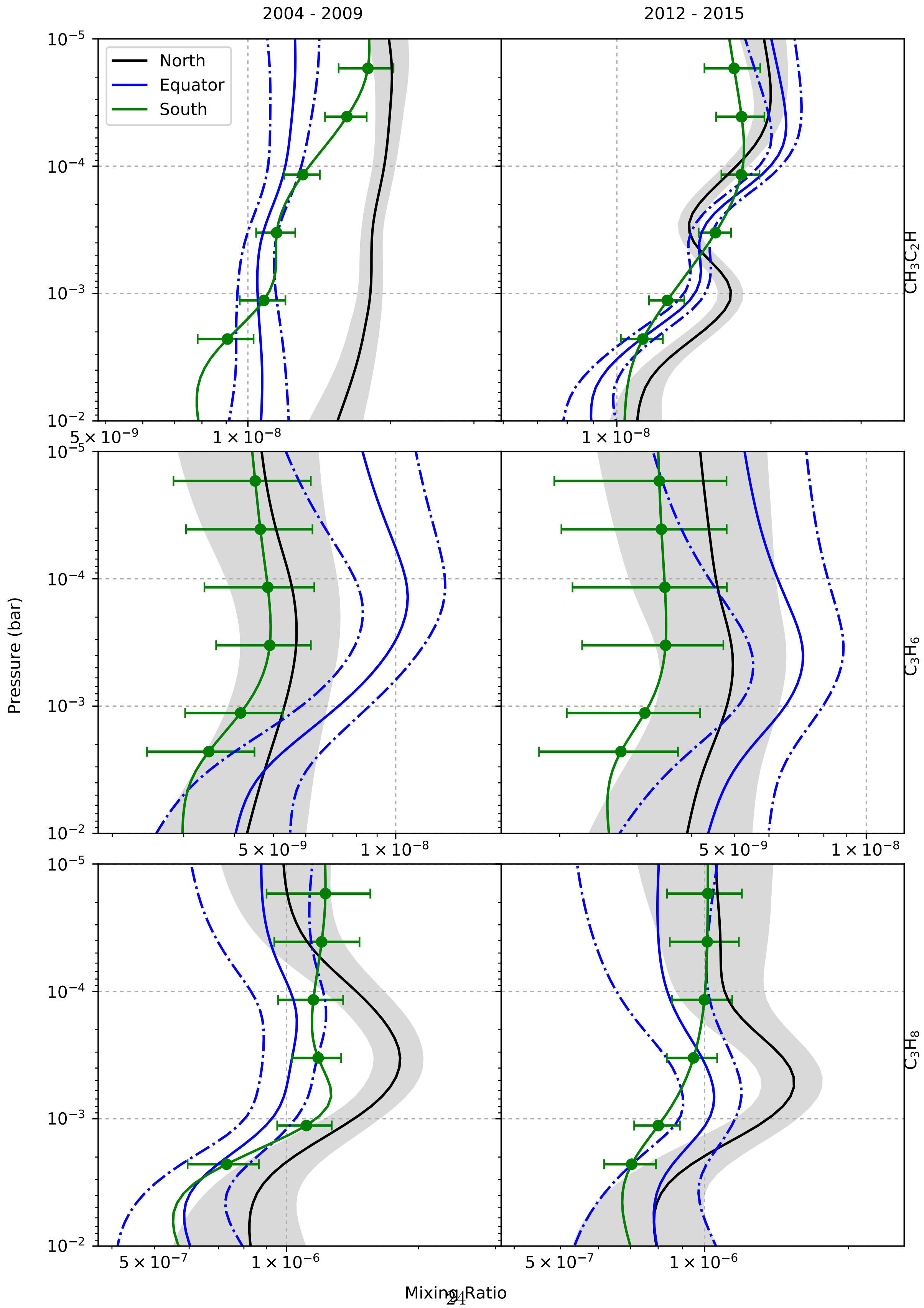

Figure 8: Vertical profiles C_3H_4(top), C_3H_6 (middle), C_3H_8 (bottom). Black is the northern bin, blue is the equatorial bin, and green is the southern bin. Volume mixing ratios are given as solid lines. 1-σ errors are given as colored regions, dot-dashed lines, or horizontal error bars at altitudes of peak contribution.

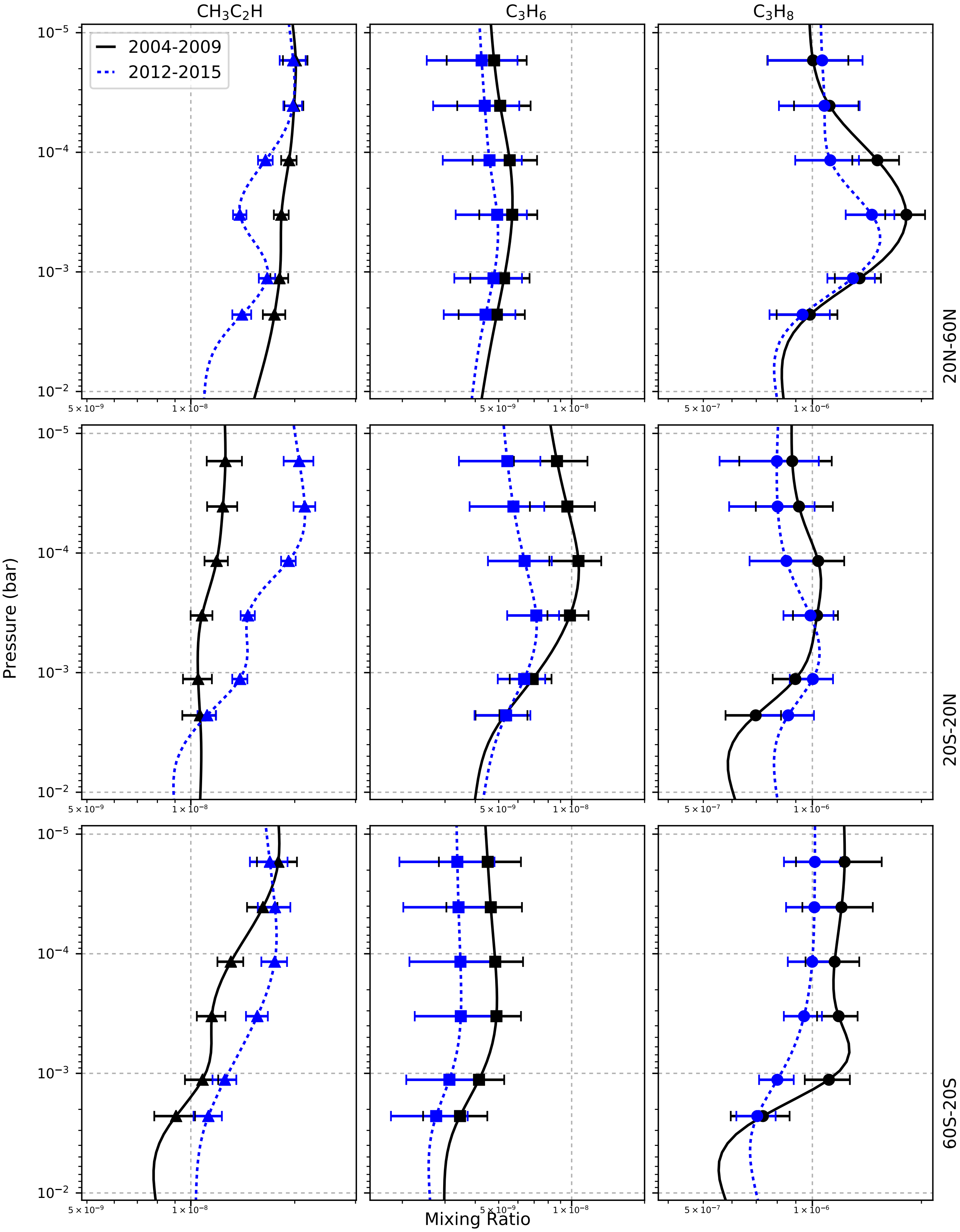

Figure 9: Vertical profiles of our retrieved gases. Volume mixing ratios for the 2004-2009 time span are solid lines and volume mixing ratios for the 2012-2015 time span are dotted lines. 1-σ errors are given as errorbars at peak contribution altitudes.

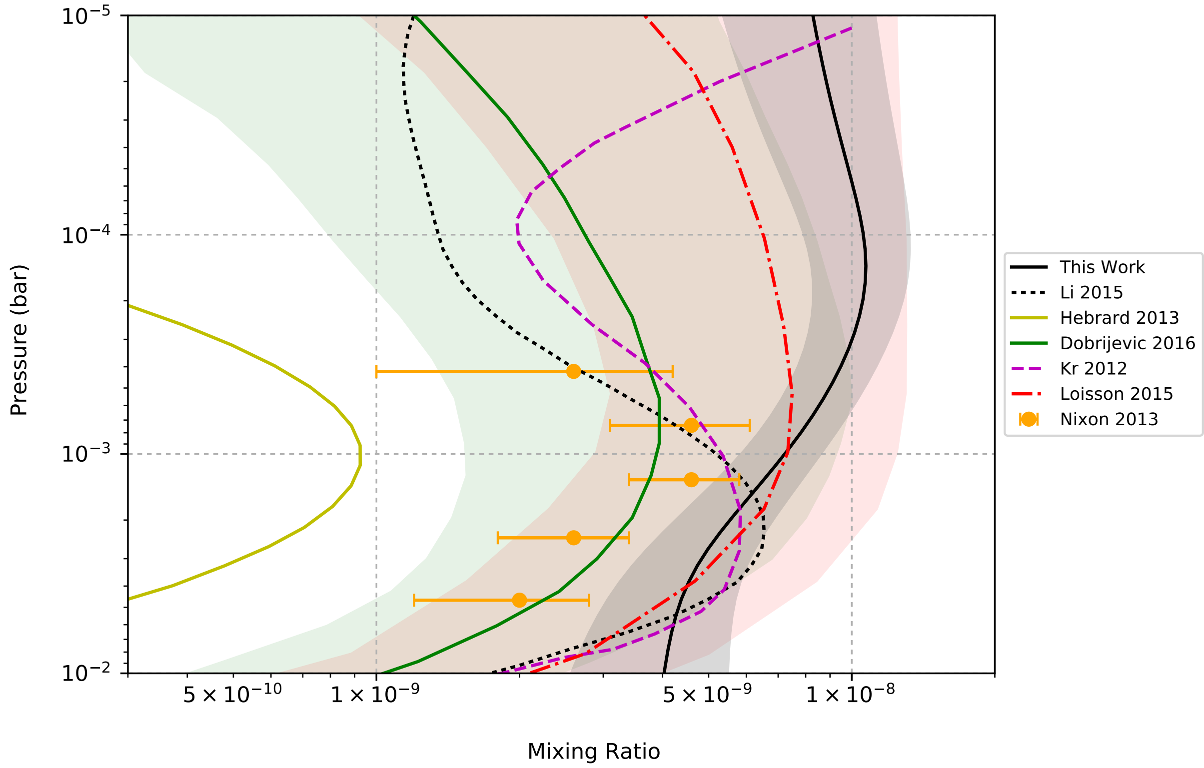

Figure 10: Our 2004-2009 20°S - 20°N profile compared with published predictions for propene's abundance. Errors on Hebrard 2013 correspond to 75th percentile, Loison 2015 correspond to 90th percentile, Dobrijevic 2016 correspond to 90the percentile. Nixon 2013 values are inferred abundances and uncertainties described in Nixon et al. (2013). Of the models compared, only Loison 2015 has a similar shape and abundance to our measured values.

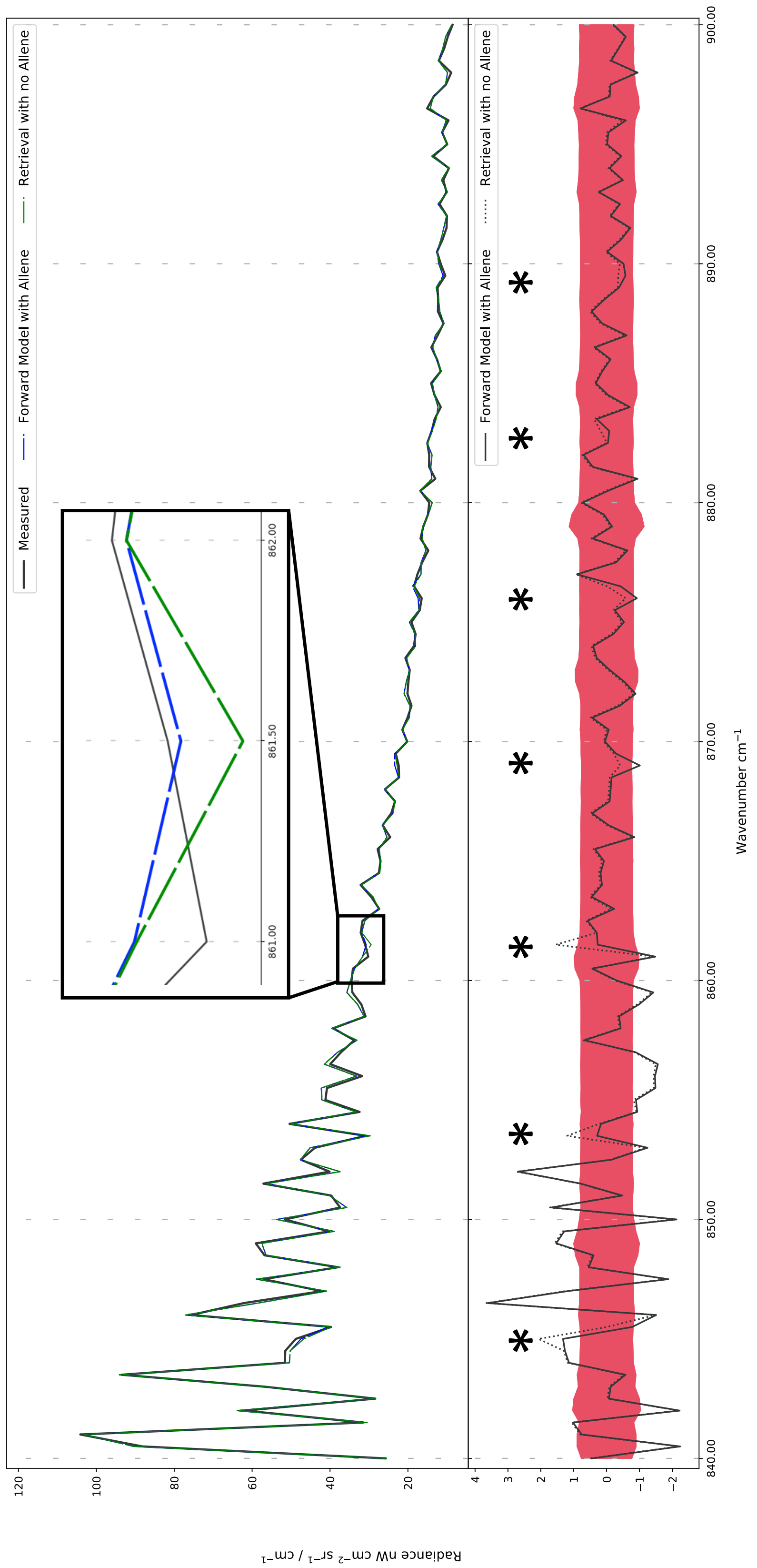

Figure 11: Comparison of modeled spectrum without allene (green) and forward modeled spectrum including allene (blue), against the observed spectrum (black). Differences in the spectra are most easily noted in the residuals, where contributions from allene are seen as peaks in the dashed spectrum, noted by asterisks.

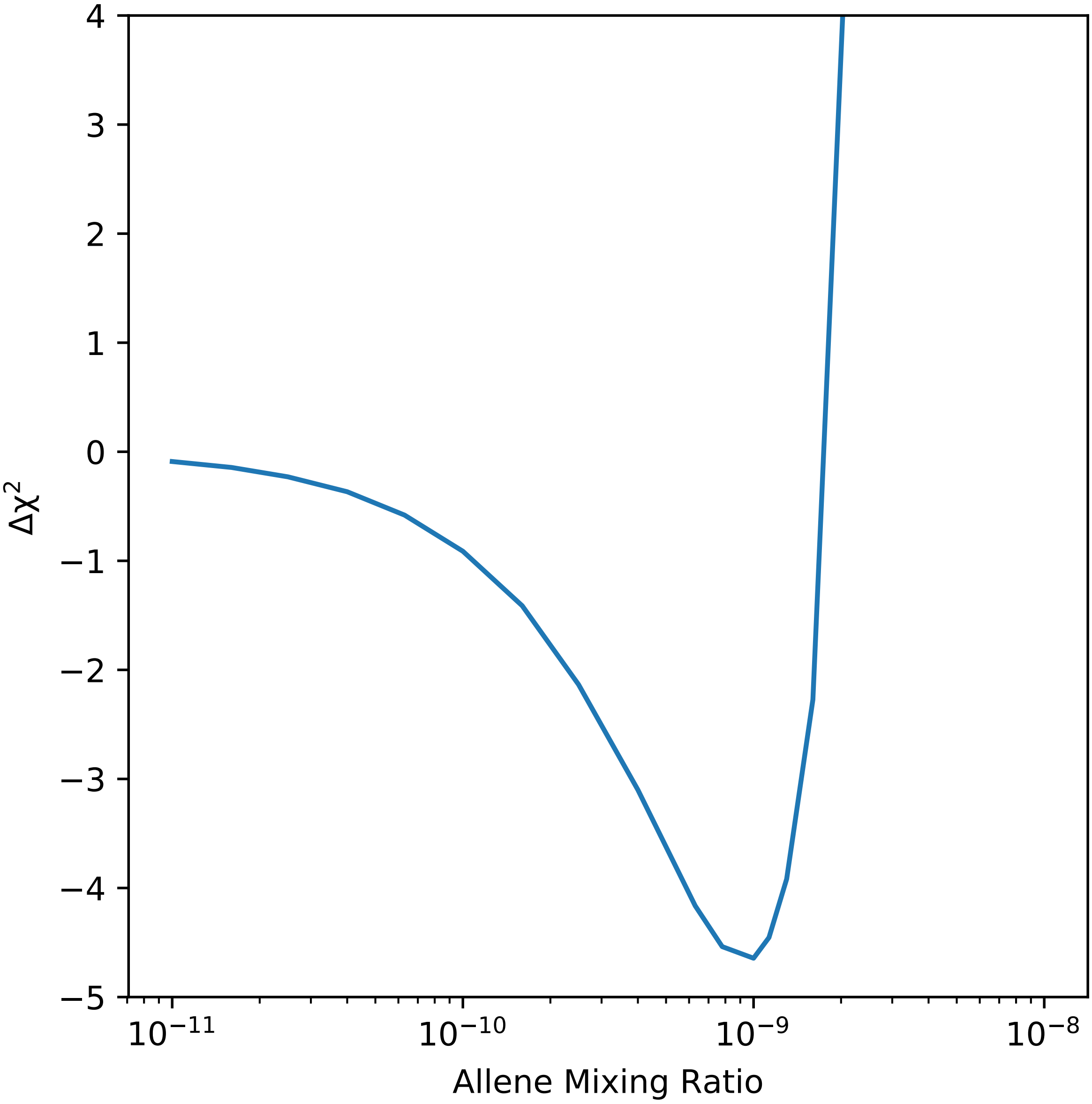

Figure 12: Plot of the $\Delta\chi^2$ against allene abundance. $\Delta\chi^2$ is calculated by subtracting the χ^2 calculated from the forward model with allene included in the atmosphere from the χ^2 value calculated from retrieved spectrum that does not include allene. Along these lines, a negative $\Delta\chi^2$ indicates the model-fit has improved, whereas a positive value indicates the fit is worsened. The minimum value is around -4.5 near 1 $\times 10^{-9}$, leading us to an estimated 2-σ upper limit of 1 ppbv.